

Time-encoded mid-infrared Fourier-domain optical coherence tomography

Ivan Zorin^{1,*}, Paul Gattinger¹, Andrii Prylepa¹, Bettina Heise¹

Research Center for Non-Destructive Testing, Science Park 2,
Altenberger Str.69, 4040 Linz, Austria
July 8, 2022

*Corresponding author: ivan.zorin@recendt.at

Abstract

In this contribution, we report on a technically simple approach to high-resolution and sensitive spectral-domain OCT imaging in the mid-infrared range. The proposed OCT system employs an InF₃ supercontinuum source; for detection, a time-encoded spectrometer based on a single InAsSb point detector is used. The developed spectrometer enables structural imaging in the spectral range from around 3140 nm to 4190 nm with a characterised sensitivity above 80 dB and an axial resolution below 8 μm . The capabilities of the system are exhibited for imaging of porous ceramic samples and transition-stage green parts fabricated using an emerging method of lithography-based ceramic manufacturing. Besides, we demonstrate the performances and flexibility of the time-encoded spectrometer by performing OCT imaging using an inexpensive low-power (average power of 16 mW above 3 μm wavelength) supercontinuum source.

Optical coherence tomography (OCT) is a well-established non-invasive and non-contact method of three-dimensional structural imaging of rather complex specimens, which has had a major impact and is primarily used in biomedical scenarios and ophthalmology [1]. Over the past few years, prospects and effectiveness of OCT beyond biomedicine [2] have been markedly amplified in terms of applied research, since the technique has been pushed to longer wavelengths – at first, to the border of the near-infrared (near-IR) range [3, 4], and then further to the mid-IR region. The most recent studies (either implemented in the direct sensing mode based on thermal detection [5, 6] or employing nonlinear conversion techniques [7, 8]) have vividly demonstrated advanced capabilities of mid-IR OCT for probing scattering media – as the magnitude of scattering decreases with increasing wavelength, it has become

possible to investigate samples formerly ineligible for testing. In this way, these reports have exposed the benefits of shifting to the mid-IR spectral window, identified potential applications, but also challenges.

As a result, nowadays, mid-IR OCT became an emerging sub-branch that has already gained significant attention in the field of non-destructive testing and defectoscopy of strongly scattering industrial samples (with potentials for applied biomedical research by escaping water absorption bands). The main obstacle that still firmly limits the efficiency and widespread implementation of OCT operating in this afresh opened spectral band is essentially technical and set by the lag in specifications of detection modalities or their technical complexity. Taking a broader perspective, it is particularly interesting that the presented mid-IR OCT systems demonstrated the boosted probing capabilities despite and against the seriously limited dynamic ranges compared to well-developed near-IR OCT counterparts. Thus, it was a primary reason to establish mid-IR OCT in the Fourier-domain (FD-OCT) configuration that has a fundamental sensitivity advantage over the time-domain (TD-OCT) [9, 10], since in the former all the depths components are being sensed simultaneously and do not contribute to depth-dependent noise as inherent in TD-OCT.

The FD-OCT configuration when migrating to the mid-IR imposes a number of realisation complications (mid-IR swept-sources are not yet mature enough). For example, unlike TD-OCT, which uses a single-point detector, the FD-OCT requires a broadband mid-IR spectrometer with well separated spectral channels that is based – in the most standard configuration – on a linear array (spectral-domain OCT, SD-OCT). Currently, modern mid-IR focal plane arrays exhibit compromised sensitivity (inherent for both – low band gap semiconductor as well as for thermal detector technologies); they are inexpediently expensive (in particular photonic systems) and have a small number of pixels (relevant for thermal systems). For this reason, the

reported mid-IR OCT realisations either exploited conversion techniques to perform detection using well-developed technologies of the near-IR range; or employed direct sensing using a pyroelectric array with proper handling of the system’s limitations. In the first case, the sensitivity of the systems has been strongly affected by the relative inefficiency of the conversion techniques; but a broad spectral range and high-performance cameras enabled a high axial resolution and reasonable sensitivity roll-off. In contrast, the direct sensing OCT based on thermal arrays provided a relatively higher sensitivity but exhibited compromised axial resolution and a strong trade-off between spatial performance and signal roll-off; here, an extension of the spectral bandwidth was not feasible causing a sharp sensitivity drop over depth, since the spectral resolution of the spectrometer becomes reduced owing to the limited number of pixels.

In this letter, we elaborate on these issues and report on a feasible design that is not only effective in terms of sensitivity, spatial and noise performance, but also technically simple and cost-effective. Thus, we propose a detection system well-suited for mid-IR OCT, which elegantly combines the benefits of both TD- and FD-OCT.

The developed time-encoded mid-IR FD-OCT system was established using standard – for an IR laboratory – on-shelf components. The principle optical layout of the setup and basic operational principles are shown in Fig. 1. The system is free-space, based on a Michelson interferometer [see Fig. 1(a)] that is formed by a pellicle beamsplitter (nitrocellulose membrane-based, BP145B4, Thorlabs) to eliminate ghost imaging artifacts; a 1-inch gold flat mirror is employed in the reference arm. In the sample arm of the interferometer, the supercontinuum beam is focused onto the sample (fixed on a three-axis motorised stage) using a standard BaF₂ singlet lens (6 mm thick, anti-reflection coated, 50 mm focal length). Due to the significantly broader operational spectral bandwidth of the developed time-encoded spectrometer, an influence of group velocity dispersion degrading the axial resolution was distinctly observed, so that a BaF₂ flat window (5 mm thick, anti-reflection coated) was inserted in the reference arm for the first-stage hardware compensation. The schema of the interferometer (except the BaF₂ window) and focusing optics has not changed from the one demonstrated in [11], hence the characterisation of lateral resolution (39 μm at 4 μm wavelength) is not provided here and the reader should refer to the aforementioned publication.

For the principal design of the key assembly, i.e. of the time-encoded dispersive OCT spectrometer, we adopted and customised the concept of a high-finesse polygon-based wavelength-scanning filter proposed in [12, 13], which was then further implemented and analysed for OCT in [14] (quite a similar idea was introduced in [15]); besides, various aspects of the employed approach have been also inten-

sively considered and discussed in [16, 17].

In order to make the system compatible and effective for mid-IR OCT imaging, refractive optics comprising a 4f system in the initial design was replaced with reflective optics. The transition is motivated by the fact that mirrors are free of chromatic aberration, which can dominate for the broad spectral range of the mid-IR OCT, thus, disturbing performances of the spectrometer; achromatic lenses in the mid-IR spectral region are still challenging – either limited in spectral bandwidth, efficiency or in aperture (aperture sizes above 1-inch are required). Hence, we employed standard spherical concave mirrors (gold, 100 mm focal length, SM1 and SM2 in Fig. 1) to form the 4f system that conjugates (in the sagittal plane, where diffraction occurs) the plane of the reflective diffraction grating (300 lines/mm) and a scanner. Instead of a polygonal scanning mirror, we utilised a galvo scanner (at rates from 25 up to 60 Hz). It was done to enhance spectral resolution and reduce potential nonlinearities, since in the polygonal mirror design the rotational axis is off of the facets, thus, introducing a jittering (beam transitions, displacements) in the sagittal plane (i.e. spectral diversification plane) during scanning. Thus, in our design, the rotational motion of the galvo mirror (conjugated to the grating, i.e. different spectral components are incident on the scanner at different angles and overlap in the plane of the scanning mirror) induces a linear spatial sweep of spectral-angular components. In other words, the scanner selects a certain wavelength over the diffraction angles by deflecting it in a certain direction. The detailed schematic drawing of the time-encoded system is shown in Fig. 1(b).

Since the spherical mirrors are employed in non-normal incidence, the system exhibits astigmatism. The effects of astigmatism do not introduce any reduction of spectral resolution as they enlarge the spot size in the plane orthogonal to the scanning plane; but they forced us to change the concept of the tunable system (initially used at the light source side to establish a swept-source using an instantaneous broadband emitter). Hence, we utilised the spectral scanner after the OCT interferometer, i.e. as a detection spectrometer. In our configuration, each spectral component selected by the scanner is focused onto a single point detector (an uncooled low-cost amplified InAsSb detector, Thorlabs PDA07P2, was employed) behind a slit (adjustable from 200 μm to 400 μm) by a long focal length spherical mirror (gold, 750 mm focal length). The focusing substantially increases the signal-to-noise ratio of the system and narrows focal spots, however, the use of long focal length optics is particularly crucial for improving spectral resolution by keeping the linear dispersion small ($\delta\lambda/\delta l$, δl is the unit length in the focal plane). In summary, in contrast to the near-IR OCT implementations, where the key advantage of the concept was increasing OCT imaging speed [14], the advantage which is provided by the tunable system in our

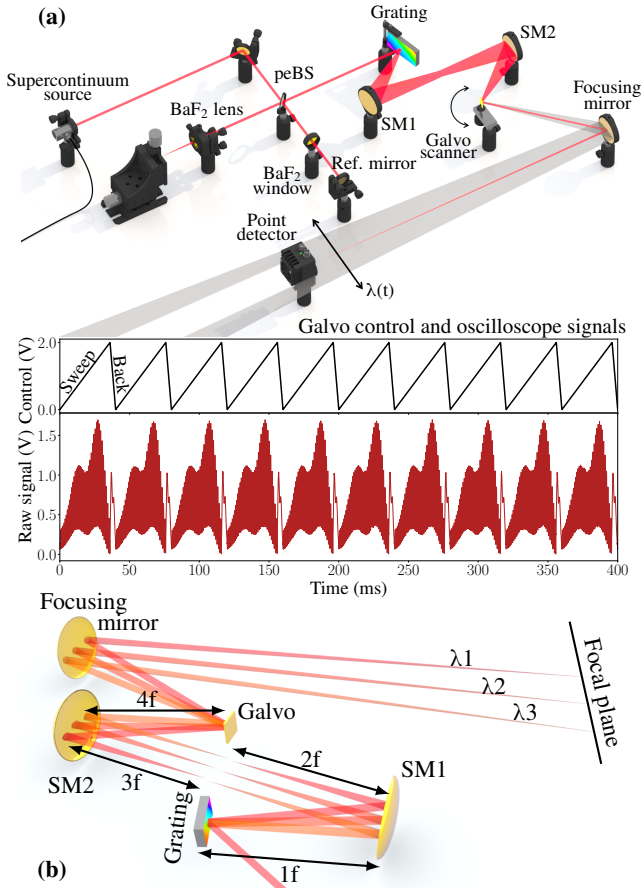


Figure 1: Basic schema (simplified) and operational principles of the time-encoded mid-IR FD-OCT system; (a) optical layout of the OCT system, peBS - pellicle beam splitter; SM1 and SM2 - the identical spherical mirrors forming 4f system to conjugate the grating and scanning planes; raw asymmetric galvo control signals and corresponding real measured spectral interferograms (for a 16 mW mid-IR supercontinuum source) are shown below; (b) enlarged and detailed optical schema of the time encoded spectrometer.

particular case, has also changed. So, on closer inspection, the time-encoded spectrometer allowed us to simply implement a virtual high-resolution mid-IR linear array (unavailable for this spectral region) with time-separated pixels (as opposed to spatial-separated pixels of cameras).

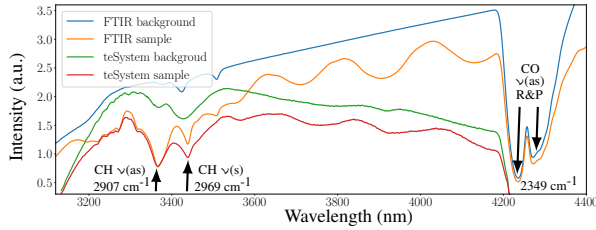
For experimental demonstrations, primarily a high-power mid-IR supercontinuum source based on a InF_3 fibre (Leukos) was used. In comparison to ZBLAN based (ZrF_4 - BaF_2 - LaF_3 - AlF_3 - NaF) supercontinuum generators, it provides a relatively flat spectral shape within a broad spectral bandwidth, thus, making it optimal for OCT. The employed source radiates around 230 mW of average optical power above 2.4 μm wavelength (spanning up to approximately 4.6 μm). The emission is pulsed (ns regime)

and features a low duty-cycle, the pulse repetition rate is 250 kHz; for this reason, a boxcar gated integrator (8 cycles averaging) was used to demodulate spectral interferograms and remove inter-pulse noises; a low-cost oscilloscope (Red Pitaya, STEMLab 125-14) was used to acquire signals. To illustrate the time-encoded system's flexibility and capabilities for OCT imaging, we also utilised a cost-effective ZBLAN based supercontinuum emitter (test system, NKT Photonics), radiating only 16 mW of average optical power above 3 μm wavelength at 40 kHz repetition rate (sub-ns regime); due to the pronounced spectral non-uniformity, a spectral bandwidth from approximately 3.4 μm to 4.1 μm was effectively used in this case.

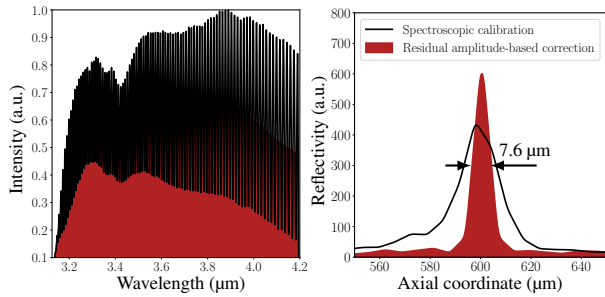
The operating spectral band of the time-encoded spectrometer was calibrated prior to performing the remapping of spectral interferograms into k -space (conceptually the same post-processing algorithm as in [5] was used). For this purpose, tools provided by mid-IR spectroscopy were exploited. Thus, sharp absorption peaks of polyethylene terephthalate (PET) caused by CH (carbon-hydrogen) bond stretching vibrations and absorption bands of carbon dioxide (CO_2) in air were used as spectral features to get a calibration vector. Reference spectral measurements were performed by a commercial high-precision Fourier-transform infrared spectrometer (FTIR, Vertex 70, Bruker Optics). The calibration function appeared to be nonlinear presumably due to the varying speed of the scanner at the beginning and end of a sweep cycle, however, the recorded spectra and fringes (phase and frequency) are highly time-repeatable and instabilities are not noticeable (i.e. nonlinearity does not fluctuate from sweep to sweep); hence, the calibration procedure has been obtained once, and the calibration vector was stored.

Figure 2(a) depicts details on the calibration procedure and spectral features used; raw spectra of the PET (also exhibit interference patterns produced by the thin film) and background spectra (sources emissions) for both: the time-encoded spectrometer (the film was inserted in the reference arm, sample arm blocked) and FTIR reference system are shown. The calibrated emission spectrum of the InF_3 supercontinuum source used for OCT and a typical spectral interferogram (for a single reflector) are shown in Fig. 2(b).

In addition to the hardware dispersion compensation, residual dispersion effects and nonlinearities were compensated numerically using a straightforward amplitude-based approach [18]. Supposing prior physical knowledge about an ideal OCT signal that fringes are equally spaced, we exploited peak positions of a reference spectral interferogram recorded for a single interface to eliminate the residual local nonlinear behaviour (similar to a zero-crossing method). The derived calibration vector was implemented into the post-processing algorithm for correction of signals in k -space. Figure 2(c) shows an obtained axial



(a) Spectroscopic calibration of the time-encoded spectrometer (teSystem) using absorption bands of a PET polymer film and CO₂ as a reference (FTIR measurements); for the sake of clarity, raw spectra shown (spectral features used for calibration highlighted)



(b) Calibrated spectral bandwidth

(c) Axial resolution characterisation

Figure 2: Performances of the time-encoded system: (a) calibration of the operational band; (b) accessed spectral bandwidth of mid-IR OCT (emission of the InF₃ fibre-based supercontinuum [Leukos]); (c) corresponding axial point spread functions.

point spread function and characterisation of axial resolution (7.6 μm). The sensitivity of the system was characterised to be 80.17 dB; low-frequency noise dominated (in the region up to around 0.4 mm, above 0.4 mm noise decreases resulting in a sensitivity of 82.92 dB); the sensitivity with the low-power source was 69.3 dB (16 μm characterised axial resolution). The noise floor was defined for a limited range of up to 6 mm.

The performance of the developed mid-IR OCT system has been validated in the attractive applied field – for structural imaging of porous industrial samples produced by an additive method of lithography-based ceramic manufacturing (LCM). Figure 3 depicts typical OCT scans of sintered highly scattering ceramic plates (approx. 325 μm and 480 μm thick). The system demonstrated enhanced probing capabilities that are common for mid-IR OCT (the morphology was not accessed by commercial near-IR OCT systems), the back interfaces of the test samples were revealed; a production curvature defect in the thin plate (325 μm) was observed. In addition, samples exhibiting another class of LCM defects were investigated. Figure 4 shows mid-IR

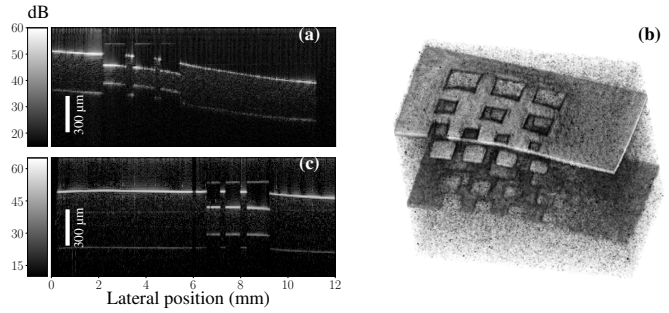


Figure 3: OCT imaging of strongly scattering ceramics (alumina, 1-2% porosity, LCM-produced, sintered at 1650°C) represented by test structured plates: 325 μm thick sample [(a) b-scan, (b) volume scan] and 480 μm [(c) b-scan scan].

OCT imaging of alumina ceramics (same material properties) with local subsurface porosity variations. The presence of short mid-IR wavelengths in the broad OCT bandwidth allowed us to gain some advantages and visualise varying scattering behaviour. Thus, depth profiles of clusters with reduced porosity were accessed; high porosity zones surrounding the clusters can be identified.

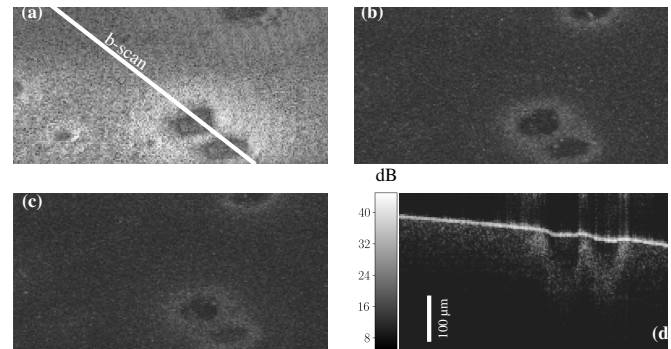


Figure 4: Sub-surface porosity heterogeneities for LCM-printed ceramics: (a-c) en-face images (10x5 mm² area) at different depths (surface, about 100 μm, 150 μm); (d) b-scan, the effective depth is limited to around 0.4 mm for the alumina group index (1.83).

Particularly interesting results were obtained for imaging of green LCM parts (intermediate production stage) using a 16 mW mid-IR supercontinuum source. The samples are strongly scattering, made of a solid flexible material that consists of ceramic particles embedded in a polymer matrix (on the basis of acrylate and methacrylate). A b-scan of the 650 μm thick green sample [corresponds to the sintered part shown in Fig. 3(b)] is depicted in Fig. 5(a). For comparison, a b-scan obtained using a state-of-the-art commercial near-IR OCT (1.3 μm center wavelength, swept-source

OCT, Vega, Thorlabs) is shown in Fig. 5(b). The recorded scans demonstrate the enhanced probing performance but also perspectives for the time-encoded mid-IR OCT based on the low-power light source; for the near-IR OCT system multiple scattering dominates, the bottom interface is not detected.

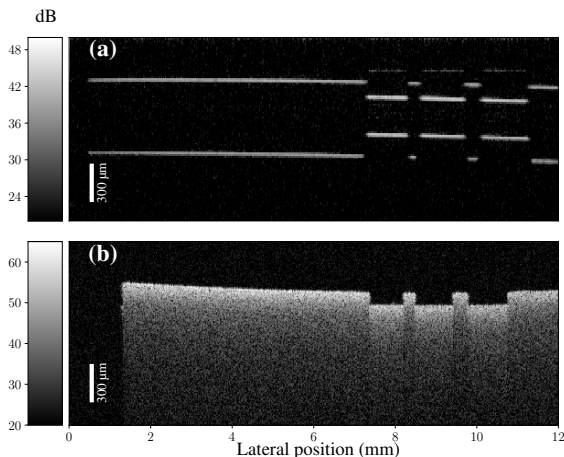


Figure 5: OCT imaging of the green LCM parts using (a) the time-encoded mid-IR OCT with the cost-effective 16 mW supercontinuum source and (b) the commercial 1.3 μm SS-OCT system.

In conclusion, we have proposed and experimentally demonstrated a simple and efficient approach to perform high-resolution mid-IR FD-OCT imaging in the direct sensing mode using time-encoded detection. The developed system combines the strengths of the TD- and FD-OCT configurations since it employs a single-point detector, but also inherits the specific sensitivity advantage through exploiting a concept of a virtual array with time-separated pixels. The experimental results have indicated practical prospects for applications in field conditions. As future work, we envisage optimising imaging speed and sensitivity using advanced detection technologies and foresee optical adaptation of the schema to improve spectral performance and possibly to establish mid-IR sweep OCT sources.

References

- [1] J. Fujimoto and E. Swanson, "The Development, Commercialization, and Impact of Optical Coherence Tomography," *Investigative Ophthalmology & Visual Science*, vol. 57, pp. 1–13, July 2016.
- [2] D. Stifter, "Beyond biomedicine: a review of alternative applications and developments for optical coherence tomography," *Applied Physics B*, vol. 88, pp. 337–357, Aug 2007.
- [3] C. S. Cheung, J. M. O. Daniel, M. Tokurakawa, W. A. Clarkson, and H. Liang, "Optical coherence tomography in the 2- μm wavelength regime for paint and other high opacity materials," *Opt. Lett.*, vol. 39, pp. 6509–6512, Nov 2014.
- [4] C. S. Cheung, J. M. O. Daniel, M. Tokurakawa, W. A. Clarkson, and H. Liang, "High resolution fourier domain optical coherence tomography in the 2 μm wavelength range using a broadband supercontinuum source," *Opt. Express*, vol. 23, pp. 1992–2001, Feb 2015.
- [5] I. Zorin, R. Su, A. Prylepa, J. Kilgus, M. Brandstetter, and B. Heise, "Mid-infrared fourier-domain optical coherence tomography with a pyroelectric linear array," *Opt. Express*, vol. 26, pp. 33428–33439, Dec 2018.
- [6] I. Zorin, P. Gattinger, M. Brandstetter, and B. Heise, "Dual-band infrared optical coherence tomography using a single supercontinuum source," *Opt. Express*, vol. 28, pp. 7858–7874, Mar 2020.
- [7] N. M. Israelsen, C. R. Petersen, A. Barh, D. Jain, M. Jensen, G. Hanneschläger, P. Tidemand-Lichtenberg, C. Pedersen, A. Podoleanu, and O. Bang, "Real-time high-resolution mid-infrared optical coherence tomography," *Light: Science & Applications*, vol. 8, pp. 2047–7538, Jan 2019.
- [8] A. Vanselow, P. Kaufmann, I. Zorin, B. Heise, H. M. Chrzanowski, and S. Ramelow, "Frequency-domain optical coherence tomography with undetected mid-infrared photons," *Optica*, vol. 7, pp. 1729–1736, Dec 2020.
- [9] R. Leitgeb, C. K. Hitzenberger, and A. F. Fercher, "Performance of fourier domain vs. time domain optical coherence tomography," *Opt. Express*, vol. 11, pp. 889–894, Apr 2003.
- [10] M. A. Choma, M. V. Sarunic, C. Yang, and J. A. Izatt, "Sensitivity advantage of swept source and fourier domain optical coherence tomography," *Opt. Express*, vol. 11, pp. 2183–2189, Sep 2003.
- [11] I. Zorin, R. Su, B. Heise, B. Lendl, and M. Brandstetter, "Correlative infrared optical coherence tomography and hyperspectral chemical imaging," *J. Opt. Soc. Am. A*, vol. 37, pp. B19–B26, Sep 2020.
- [12] S. H. Yun, C. Boudoux, G. J. Tearney, and B. E. Bouma, "High-speed wavelength-swept semiconductor laser with a polygon-scanner-based wavelength filter," *Opt. Lett.*, vol. 28, pp. 1981–1983, Oct 2003.

- [13] W. Y. Oh, S. H. Yun, G. J. Tearney, and B. E. Bouma, "115 khz tuning repetition rate ultrahigh-speed wavelength-swept semiconductor laser," *Opt. Lett.*, vol. 30, pp. 3159–3161, Dec 2005.
- [14] W.-Y. Oh, B. J. Vakoc, M. Shishkov, G. J. Tearney, and B. E. Bouma, "400 khz repetition rate wavelength-swept laser and application to high-speed optical frequency domain imaging," *Opt. Lett.*, vol. 35, pp. 2919–2921, Sep 2010.
- [15] A. L. Oldenburg, J. J. Reynolds, D. L. Marks, and S. A. Boppart, "Fast-fourier-domain delay line for in vivo optical coherence tomography with a polygonal scanner," *Appl. Opt.*, vol. 42, pp. 4606–4611, Aug 2003.
- [16] M. Everson, V.-F. Duma, and G. Dobre, "Aspects of vignetting in a polygon mirror-based spectral filter for swept source optical coherence tomography (SS-OCT)," in *Seventh International Conference on Lasers in Medicine* (C. T. M.D., A. Podoleanu, and V.-F. Duma, eds.), vol. 10831, pp. 98 – 106, International Society for Optics and Photonics, SPIE, 2018.
- [17] M. Everson, V.-F. Duma, and G. Dobre, "Optimisation of a polygon mirror-based spectral filter for swept source optical coherence tomography (SS-OCT)," in *2nd Canterbury Conference on OCT with Emphasis on Broadband Optical Sources* (A. Podoleanu and O. Bang, eds.), vol. 10591, pp. 180 – 186, International Society for Optics and Photonics, SPIE, 2018.
- [18] M. Duelk and K. Hsu, "SLEDs and Swept Source Laser Technology for OCT," in *Optical Coherence Tomography* (W. Drexler and J. G. Fujimoto, eds.), pp. 527–561, Cham: Springer International Publishing, 2015.